

# Optimal Control of One-Dimensional Model of Stator Flow Using Air Injection Method

Nhan T. Nguyen\*

*NASA Ames Research Center, Moffett Field, CA 94035*

Michelle M. Bright<sup>†</sup>

Dennis Culley<sup>‡</sup>

*NASA Glenn Research Center, Cleveland, OH 44135*

This paper presents a model-based optimal flow control method for controlling flow separation in a stator cascade of a low-speed axial-flow compressor using an air injection technique. The objective of the flow control method is to reduce the total pressure loss across a blade row which can be viewed as an indicator of flow separation. A multi-sensor, multi-actuator flow control concept is introduced to control the total pressure profile at the outlet of the stator cascade. The flow passage is divided into a number of radial blade stations at which total pressure sensors are placed at the inlet and outlet of the stator cascade to measure the total pressure losses. This information is then used in the flow control design to determine a suitable air injection mass flow command for each individual air injection actuator. The control method is based on a one-dimensional unsteady flow model incorporating an empirical total pressure loss parameter to account for the real flow effect. The total pressure loss parameter is determined from an adaptive parameter estimation process using a recursive least-squares algorithm to enable the flow control to adapt to changing inlet flow conditions. An adjoint-based optimal control law is derived to enable a feedback flow control that tracks a reference command of the air injection mass flow in the presence of disturbances due to changing inlet flow conditions. A numerical simulation demonstrates the effectiveness of the proposed flow control strategy.

## I. Introduction

An aircraft gas turbine engine comprises several major aero-mechanical components including compressors, combustors, and turbines. Within a compressor stage, stator and rotor cascades provide alternate flow passages through which a diffusion process takes place that results in an increase in the static pressure. Under critical operating conditions such as those during takeoff and landing, mass flow deficit or inlet distortion may result. As a consequence, the incidence angle on the blade row may increase substantially beyond an acceptable limit, thus causing stall and flow separation. This is as illustrated in Fig. 1, which shows an increase in the relative air inlet angle corresponding to a reduced axial flow speed. At an extreme incidence angle, air flow over the blade surface becomes detached and forms blockage regions of low velocity. The resulting flow separation may endanger safe operation of a gas turbine engine since it may induce aeromechanical instabilities such as blade stall flutter in addition to reduced compression ratios.

In modern gas turbine engines, a stall margin is normally incorporated into a design process to safeguard an engine from operating too close to a stall or surge line. Fig. 2 illustrates a stall margin on a pressure rise vs. mass flow diagram. The stall margin design directly affects the performance of a compression system since generally the pressure ratio reduces as the stall margin increases. Conversely, operating at a reduced stall margin would tend to increase a stage pressure ratio, but this potential benefit is well offset by an increased exposure of rotor blades to high cycle fatigue that can compromise the blading structural integrity. With the current advances in flow control, the ability to operate a compression system at a reduced stall margin may be realized that could potentially lead to performance improvements in the design and operation of compression systems without safety compromises due to flow separation.<sup>1</sup>

\*Computer Scientist, Intelligent Systems Division, Mail Stop 269-1

<sup>†</sup>Research Engineer, Control and Dynamics Technology Branch, Mail Stop 77-1

<sup>‡</sup>Research Engineer, Control and Dynamics Technology Branch, Mail Stop 77-1

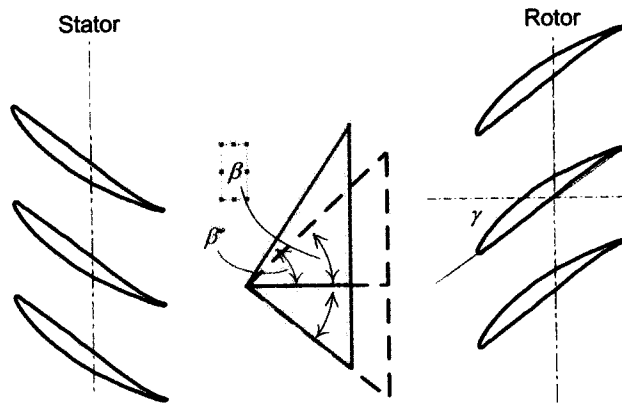


Fig. 1 - Incidence Angle Change from Mass Flow Deficit

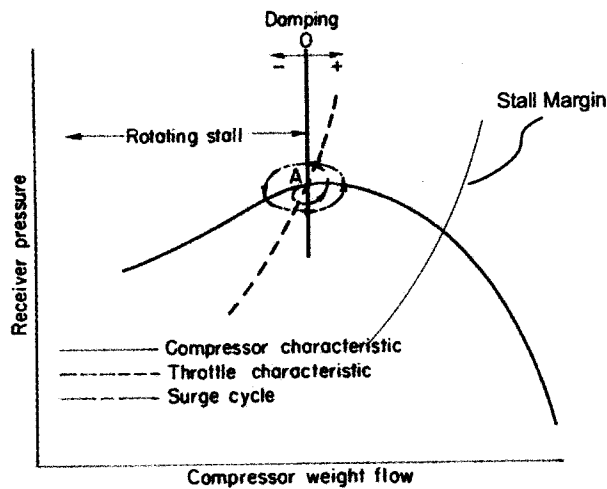


Fig. 2 - Stall Margin

Compressor flow control methods have been investigated by many researchers and there exists a large body of knowledge pertaining to this area of research.<sup>2,3</sup> One well-known method is to inject bypassed mass flow from the downstream into the upstream face of the compressor to make up for the mass flow deficit that causes flow separation.<sup>4</sup> Another method which has been evaluated by NASA Glenn Research Center is to use air injection on the surface of stator vanes for controlling flow separation within a stator cascade.<sup>5</sup> Many similar techniques also exist using synthetic jet actuators.<sup>6</sup> The air injection flow control is based on a well-known fluid physics principle which shows that the growth of a boundary layer that causes flow separation can typically be suppressed by a high momentum small-scale flow, which helps energize the low momentum air accumulated near the blade suction surface by promoting fluid momentum exchange. An experiment has been conducted in the Low Speed Axial-Flow Compressor (LSAC) test facility at NASA Glenn Research Center to investigate the effectiveness of this flow control method. Test data have confirmed that this method is capable of reducing flow blockage formed within a stator cascade in the LSAC using both steady and unsteady air injection.<sup>5</sup>

The flow control vanes are fabricated to incorporate a series of air injection slots on the suction surface to provide a coverage from approximately 10% to 90% of span as shown in Fig. 3. The blade section is a modified NACA 65-series airfoil with a circular-arc mean camber line. The optimal air injection location is at 35% of chord as determined in a wind tunnel study performed by the Illinois Institute of Technology.<sup>5</sup> In all vane configurations, the injection angle is pitched at 30° relative to the vane upper surface to impart a streamwise momentum to the flow.

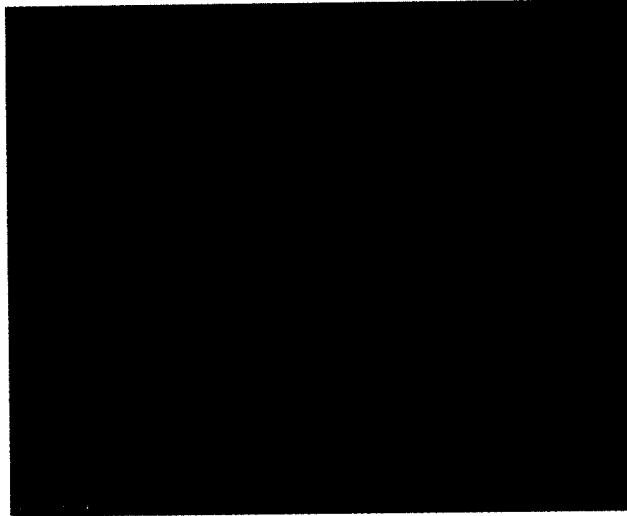


Fig. 3 - Flow Control Stator Vane

Fig. 4 shows the LSAC test facility. The LSAC compressor is driven by a 1,500-hp variable speed motor and consists of a row of inlet guide vanes and four identical stages designed for accurate low-speed simulation of the rear stages of a high-speed core compressor. With reference to Fig. 5, the first two stages are used to set up a repeating stage environment. The third stage is the focus of research measurements, while the fourth stage acts as a buffer to the exit conditions. The flow path has an outer diameter of 1.219 m and a hub-to-tip radius ratio of 0.80. The nominal rotor tip and stator seal clearances are 1.4% and 0.6% of span respectively. Rotor tip speed is 61 m/sec and nominal axial velocity is on the order of 25 m/sec.

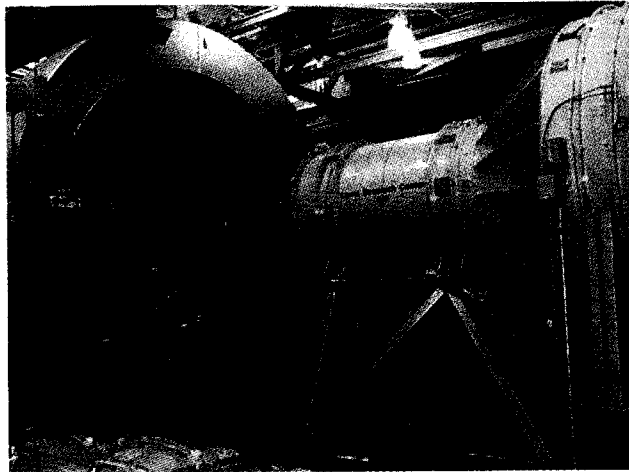


Fig. 4 - NASA Glenn Low Speed Axial-Flow Compressor (LSAC) Test Facility

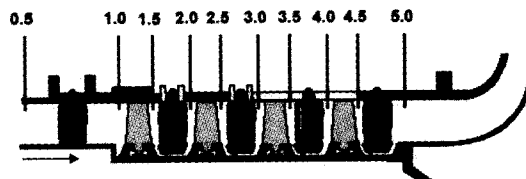


Fig. 5 - Compressor Stages

The LSAC experiment has been conducted in an open-loop mode, but feedback flow control has not been implemented. Feedback flow control is generally more challenging since the air injection mass flow must be determined as a function of a suitable state variable that would bring about a desired effect. The goal of this study is to develop a feedback flow control method that reduces the total pressure loss across a blade row which is viewed as a reliable indicator of flow separation. The approach employed in this study is based on a reduced-order fluid dynamics model using the one-dimensional unsteady momentum equation for compressible flow to model the circumferential average two-dimensional flow through the cascade. The radial profile of the flow is controlled by placing multiple sensors and actuators on a number of radial stations. A total pressure loss parameter is incorporated into the momentum equation to represent the effect of the total pressure loss due to flow separation. An adjoint-based optimal control for this one-dimensional flow model is developed to provide a feedback control law that can handle disturbances due to changing inlet flow conditions. A simulation is conducted and demonstrates the effectiveness of the proposed flow control method.

## II. Experimental Data Analysis

The LSAC is equipped with flow instrumentation to measure average pressure rise coefficients from inlet and outlet static pressure measurements on the hub and casing. The flow coefficient is defined as the measured mean inlet velocity normalized by the rotor tip speed. The mean inlet velocity is determined from static pressure measurements at the exit of the inlet bell mouth using a discharge coefficient corrected for humidity. The flow control vane performance is calculated from total pressure measurements acquired with miniature Kiel probes and static pressure. The flow angle measurements are acquired with  $18^\circ$  wedge probes. All pressure measurements are acquired at mid-gap of the rotor-stator spacing (the spacing is approximately 35% of axial chord) and are referenced to stagnation conditions measured in the inlet plenum of the test facility.

The LSAC experiment was set up to have two flow control vanes placed in between conventional stator vanes. In order to induce flow separation, the flow control vanes were re-staggered by  $-3^\circ$  from the nominal setting. The data were acquired by a slow speed 1-Hz traversing probe that surveys the pressure profiles over one flow control vane and one conventional stator vane at the upstream and downstream sides. The total pressure profiles at the upstream and downstream of the conventional and flow control vanes and the air injection mass flow schedule are plotted in Figs. 6 and 7.

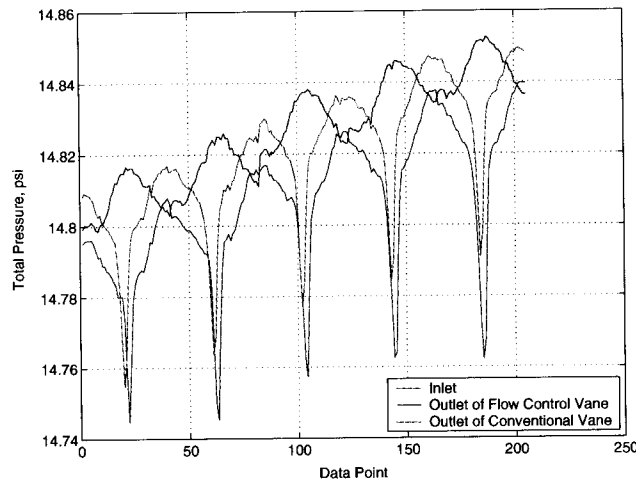


Fig. 6 - Total Pressure Measurements

The data are plotted contiguously for five different runs, each run corresponds to a different steady air injection mass flow as shown in Fig. 7. The data points represent the position of the traversing probe over one blade spacing interval. We see from Fig. 6 that the total pressure at the outlet of the flow control vane is paradoxically lower than that at the outlet of the conventional stator vane. This is simply due the fact that, in order to induce flow separation, the flow control vanes were re-staggered to a higher incidence angle by  $-3^\circ$  from the nominal setting of the conventional

stator vanes. As a result, the total pressure loss for the flow control vane prior to the air injection was greater than that for the conventional stator vane. As the steady air injection mass flow reduces, the total pressure wake at the outlet grows in amplitude. Fig. 8 is a plot of the local total pressure loss coefficient for the flow control vane, showing a definitive trend of decreasing total pressure loss with increasing air injection mass flow.

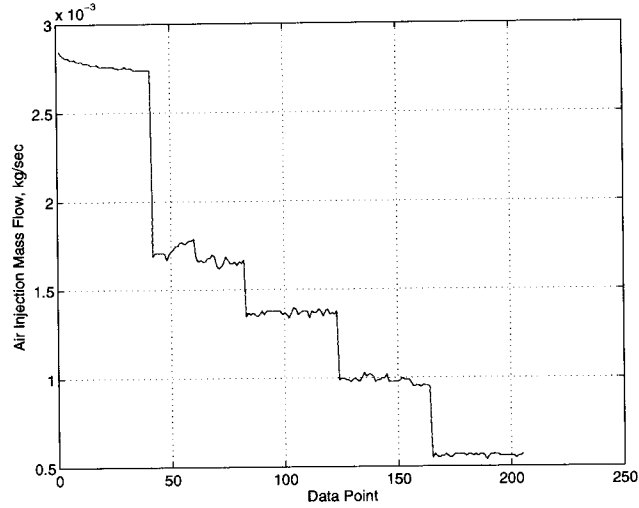


Fig. 7 - Steady Air Injection Mass Flow

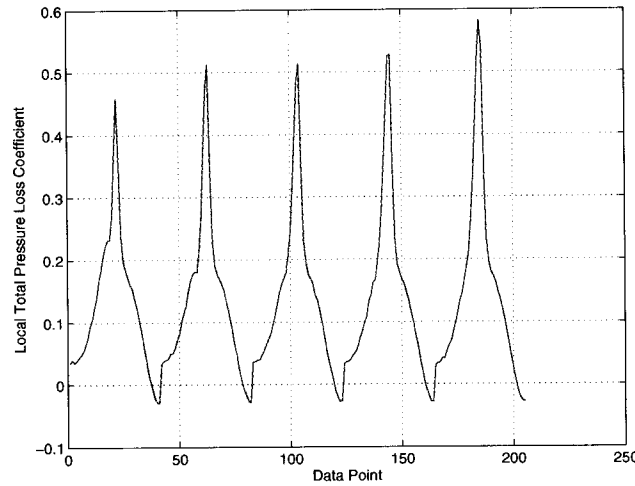


Fig. 8 - Local Total Pressure Loss Coefficient for Flow Control Vane

The total pressure data are averaged over each run corresponding to each steady air injection mass flow and are used to compute the average total pressure loss coefficient defined as

$$\bar{\omega}_1 = \frac{p_{0,1} - p_{0,2}}{p_{0,1} - p_1} \quad (1)$$

where  $p_0$  is the average total pressure,  $p$  is the average static pressure, and the subscripts 1 and 2 henceforth denote the inlet and outlet respectively.

Fig. 9 is a plot of the average total pressure loss coefficient as a function of the air injection mass flow. It clearly illustrates the effectiveness of the air injection on controlling the total pressure loss. The y-intercept of Fig. 9 represents the baseline pressure loss coefficient without air injection, which has a value of 0.1743 based on a second

degree polynomial extrapolation. We observe that the air injection control effectiveness seems to have reached a saturation limit at about  $2.5 \times 10^{-3}$  kg/sec. Further increase in the air injection mass flow beyond this value seems to result in a diminishing reduction in the total pressure loss coefficient.

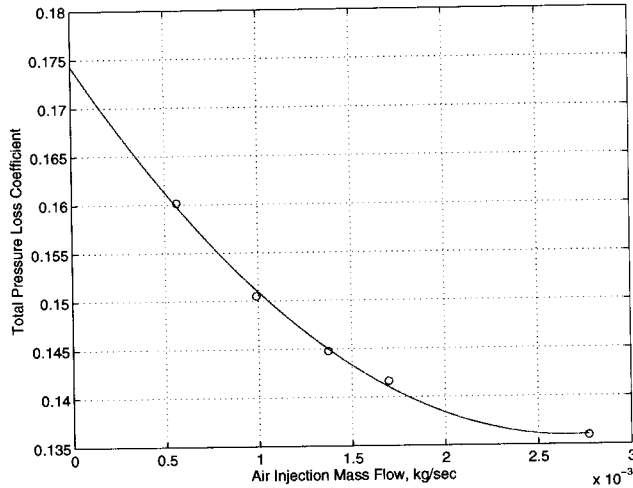


Fig. 9 - Average Total Pressure Loss Coefficient vs. Air Injection

### III. Diffusion Concept

The manifestation of flow separation generally results in flow blockage associated with rotating stall for a rotor cascade. Fig. 10 illustrates a simplified mechanism of a rotating stall in a cascade.<sup>9</sup> Initially, one of the blades in the cascade reaches a stall condition first. This stalled flow effectively forms a region of retarded flow that blocks the air from entering the flow passage around this blade. Consequently, the flow has to be diverted to other neighboring blades. The net result is that the incidence angle increases on those blades below and decreases on those blades above the retarded flow region according to Fig. 10. Consequently, the blades below become stalled while the blades above become unstalled. This stall pattern moves from the pressure side to the suction side of each blade and rotates with the rotor; hence the term rotating stall.

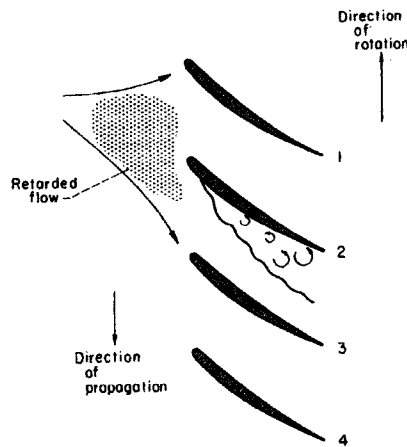


Fig. 10 - Rotating Stall Mechanism<sup>9</sup>

The stall mechanism on a blade also manifests itself as a fluid-structure interaction within a cascade. As a blade section reaches a stall point, the aerodynamic damping becomes negative as illustrated in Fig. 2. This negative

aerodynamic damping acts to reduce the overall blade damping. Consequently, the stalled blade typically experiences an increase in the structural vibration. The unsteady motion of the vibrating blade thereby causes the flow field to oscillate. As a result, the stalled flow is highly unsteady.

In diffusing flow, stall often occurs due to the presence of an adverse pressure gradient. A stalled flow usually manifests itself as a reduced static pressure recovery and an increase in the total pressure loss.<sup>8</sup> Thus, the total pressure loss can be seen as an indicator for stall or flow separation. Lieblein showed that the stall onset relates to a parameter known as a diffusion factor which is well correlated with the boundary layer wake momentum thickness in the minimum-loss region of a two-dimensional compressor cascade.<sup>9</sup> A local diffusion factor  $D_{loc}$  is defined as the ratio of the velocity difference between the maximum velocity  $V_{max}$  and the outlet velocity  $V_2$  to the maximum velocity on the suction surface

$$D_{loc} = \frac{V_{max} - V_2}{V_{max}} \quad (2)$$

Typically, a detail knowledge of the velocity distribution on a compressor blade section is usually not known, so Lieblein alternatively defined a more convenient form of the diffusion factor based on the inlet and outlet velocities of the cascade according to

$$D = \left(1 - \frac{V_2}{V_1}\right) + \frac{\Delta V_\theta}{2\sigma V_1} \quad (3)$$

where  $D$  is the diffusion factor,  $\sigma$  is the solidity,  $\Delta V_\theta$  is the change in the tangential velocity through the cascade.

For an incompressible 2-D cascade, Eq. (3) becomes

$$D = \left(1 - \frac{\cos\beta_1}{\cos\beta_2}\right) + \frac{\cos\beta_1}{2\sigma} (\tan\beta_1 - \tan\beta_2) \quad (4)$$

where  $\beta$  is the air angle.

A theoretical analysis of an incompressible two-dimensional cascade<sup>9</sup> shows that the wake momentum thickness  $\theta^*$  correlates well with the total pressure loss coefficient  $\bar{\omega}_1$  based on the inlet condition according to the relationship

$$\bar{\omega}_1 = 2 \left(\frac{\theta^*}{c}\right)_2 \frac{\sigma}{\cos\beta_2} \left(\frac{\cos\beta_1}{\cos\beta_2}\right)^2 \left\{ \frac{\frac{2H_2}{3H_2-1}}{\left[1 - \left(\frac{\theta^*}{c}\right)_2 \frac{\sigma H_2}{\cos\beta_2}\right]^3} \right\} \quad (5)$$

where  $p_0$  is the total pressure,  $\theta^*/c$  is the ratio of the wake momentum thickness to blade chord, and  $H_2$  is the wake form factor.

Hence, an increase in the wake momentum thickness resulting from flow separation in the cascade directly translates into an accompanied increase in the total pressure loss. Fig. 11 obtained from NASA SP-36 report<sup>9</sup> illustrates the diffusion factor correlation for a two-dimensional NACA 65-(A<sub>10</sub>)10 low-speed compressor cascade.

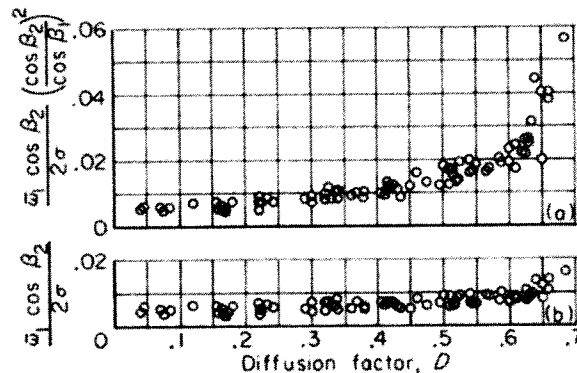


Fig. 11 - Diffusion Factor Correlation<sup>9</sup>

As illustrated in Fig. 11, the diffusion factor is correlated well with the total pressure loss coefficient as defined in Eq. (5). Lieblein showed that the total pressure loss coefficient is generally a reliable indicator of the momentum thickness of the boundary layer formed over the blade surface. Thus, the larger the total pressure loss coefficient is, the thicker the boundary layer becomes. It is generally accepted that the diffusion factor should be kept at or below 0.55 to maintain a stall-free operation. Above a diffusion factor of 0.6, the total pressure loss begins to increase rapidly<sup>9</sup> due to the thickening of the boundary layer as the flow begins to separate as shown in Fig. 11.

Based on the diffusion concept, it is reasonable to say that controlling flow separation is tantamount to controlling the total pressure loss. The most direct effect of this total pressure loss control is an increase in the static pressure recovery in a diffusing flow through the stator cascade. More importantly, this control also brings about a reduction in the boundary layer thickness, which therefore increases the turning angle and hence decreases the angle of attack on the rotor blade row to alleviate the stalled flow on the rotor.

Thus, in a compressor environment, the total pressure measurement across a blade row can provide an indication of the potential stall onset. Typically, designers should know the design total pressure loss across a blade row, which could also be measured directly by running the compressor at the design point. When operating substantially above this design value, for example twice the design loss, an inference could be made about a probable flow separation event in the compressor that needs to be corrected. Flow control vanes can then be activated to inject bleed air into the flow passage in order to bring about a reduction in the total pressure loss.

## IV. Flow Control Modeling

### A. Flow Control Concept

In this study, a model-based flow control approach is proposed for controlling the total pressure loss across a stator cascade equipped with flow control vanes. The flow control architecture incorporates an adaptive parameter estimation that can estimate on-line the relationship between the air injection mass flow and the total pressure loss under varying engine operating environment. In the current flow control concept, the air injection slots admit equal mass flow that depends on sensing at a particular radial station along the flow control vanes. The total pressure loss information at this blade station can then be used in a feedback control design for the air injection. Because the total pressure loss information comes from a single blade radial station, therefore, in theory, we could design a worst-case control whereby the sensors could be placed at the tip radius where the viscous loss is expected to be the most severe. Alternatively, we may consider a multi-sensor, multi-actuator approach that would extend the capability of the current flow control concept for situations such as inlet flow distortion whereby flow uniformity at the outlet of the stator cascade is desired. Fig. 12 illustrates a multi-sensor, multi-actuator control approach. In the limit, this flow control concept can be used for the LSAC flow control experiment that employs a single air injection actuator.

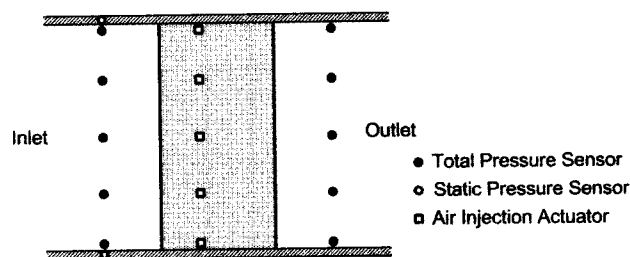


Fig. 12 - Flow Control Concept

Total pressure sensors at the inlet and outlet provide measurements of the total pressure loss across the stator cascade. The sensors may be mounted on a rake apparatus. Kiel-type sensors are well suited for total pressure measurements in the presence of flow angularity. Static pressure measurements are provided by wall static taps. The local total pressure loss coefficient can then be computed by linear interpolation of the static pressure values at the end walls. These local total pressure loss coefficients are compared to limiting values corresponding to a baseline design stall margin based on experimental measurements or aerodynamic cascade analyses. When the cascade operates beyond the baseline design stall margin, air injection actuators are activated by the flow control to maintain a desired

outlet total pressure set point in order to keep the local total pressure loss coefficients at or below the limiting values. Fig. 13 illustrates a simplified block diagram of the flow control concept.

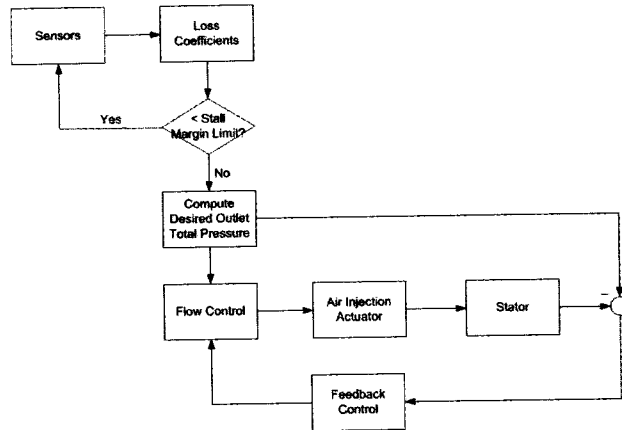


Fig. 13- Flow Control Block Diagram

### B. 1-D Curvilinear Unsteady Linearized Euler Equation

Flow through a compressor cascade is generally unsteady, viscous, and three-dimensional as the flow field varies in both the meridional and tangential planes. In addition to the main flow in the inviscid core, significant secondary flow fields near the hub and tip regions also exist. Local flow fields around blade sections resulting from the potential effect at the leading edge and the wake effect at the trailing edge create tangential variations in the global flow field. Turbomachinery flow therefore is a very complex problem to analyze even with today's available computational fluid dynamics (CFD) tools. In spite of the complexity, traditional compressor design methodologies often rely on simplified analyses that address the dominant features of the flow field. Secondary effects such as boundary layer blockage, tip clearance flow, and viscous losses are addressed in the design processes by simplified analytical and/or empirical methods. One such simplification is to ignore the flow field tangential variation in the bladeless region, thereby resulting in an axisymmetric flow field assumption which has been frequently used in the compressor design processes.<sup>10</sup> The flow properties in an axisymmetric flow field therefore can be interpreted in a circumferential average sense.

For this application, we employ a model-based flow control approach whereby feedback control laws are based on a physical model of a simplified flow through a stator cascade. Towards this end, we approximate the two-dimensional flow on a cylindrical surface through a compressor cascade as a one-dimensional curvilinear flow through a curved, diffusing flow passage defined by the stagnation streamlines as illustrated in Fig. 14. In effect, the one-dimensional flow model can be viewed as a reduced-order model of a two-dimensional flow and represents an average flow through the cascade at any given cross section normal to the flow passage. Reduced-order modeling has been frequently used in flow control applications<sup>11</sup> in recognition that a reduced fidelity of the flow field modeling is necessary in order to increase the computational speed that is needed for a real-time control application. Thus, the three-dimensional flow field is decomposed into a finite numbers of one-dimensional curvilinear flow fields at the radial stations where the sensors and air injection actuators are placed. The one-dimensional flow field is governed by the one-dimensional unsteady Euler equations with a total pressure loss parameter that accounts for the viscous dissipation of a real fluid caused by flow separation. This parameter is estimated by an adaptive parameter estimation process as a function of the air injection mass flow control, so in effect this parameter provides a means to incorporate the real-flow effect into the analytical model.

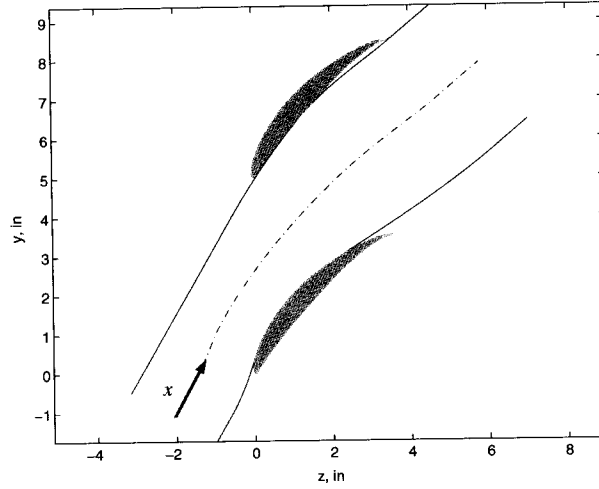


Fig. 14 - Flow Through a Compressor Cascade

For one-dimensional unsteady flow at a given blade radial station, we formulate the following Euler equations in the non-conservation form<sup>12</sup> in terms of the three compressor performance variables, namely, the mass flow  $\dot{m} = \rho u A$ , the total pressure  $p_0$ , and the total temperature  $T_0$

$$\mathbf{y}_t + \mathbf{A}(\mathbf{y}, x) \mathbf{y}_x + \mathbf{B}(\mathbf{y}, x) \boldsymbol{\xi}(x, \mathbf{v}) = \mathbf{0} \quad (6)$$

where  $\mathbf{y}(x, t) = \left[ \dot{m} \quad p_0 \quad T_0 \right]^T$  is a vector of flow variables,  $\mathbf{v} = \left[ v_1 \quad v_2 \quad \cdots \quad v_N \right]$  is an air injection mass flow control vector, and

$$\mathbf{A} = \begin{bmatrix} u & \frac{\rho A}{\rho_0} & \frac{\dot{m} u}{2T_0} \\ \frac{\rho_0 c^2}{\rho A} & u \left[ 1 - \frac{(\gamma-1)T}{T_0} \right] & \frac{\rho_0 c^2 u}{T_0} \\ \frac{(\gamma-1)T}{\rho A} & -\frac{(\gamma-1)^2 T u}{k p_0} & u \left[ 1 + \frac{(\gamma-1)T}{T_0} \right] \end{bmatrix} \quad (7)$$

$$\mathbf{B} = \begin{bmatrix} \frac{\dot{m} u}{2L} \\ \frac{\rho_0 u^3}{2L} \left( \frac{T_0}{T} - \gamma + 1 \right) \\ -\frac{(\gamma-1)uT}{L} \left( \frac{T_0}{T} - 1 \right) \end{bmatrix} \quad (8)$$

where  $\rho$  is the density,  $\rho_0$  is the total density,  $T$  is the temperature,  $p$  is the pressure,  $u$  is the flow speed,  $c$  is the speed of sound,  $\gamma$  is the specific heat ratio,  $A(x)$  is the normal flow area as a function of the curvilinear coordinate  $x$ ,  $L$  is the flow passage length, and  $\boldsymbol{\xi}$  is the total pressure loss parameter as a function of the air injection mass flow control vector  $\mathbf{v}$  as well as the curvilinear coordinate  $x$ .

For a rotor cascade, we can replace the total pressure  $p_0$ , the total temperature  $T_0$ , and the Mach number  $M$  with the relative total pressure  $p_{0,R}$ , the relative total temperature  $T_{0,R}$ , the relative Mach number  $M_R$

$$p_{0,R} = p \left( 1 + \frac{\gamma-1}{2} M_R^2 \right)^{\frac{\gamma}{\gamma-1}} \quad (9)$$

$$T_{0,R} = T \left( 1 + \frac{\gamma-1}{2} M_R^2 \right) \quad (10)$$

$$M_R^2 = M^2 + \frac{r\Omega (r\Omega - 2u_\theta)}{c^2} \quad (11)$$

where  $r$  is the blade span radius,  $\Omega$  is the rotor speed, and  $u_\theta$  is the absolute tangential velocity.

The steady state form of Eq. (6) is

$$\frac{d\mathbf{y}}{dx} = -\mathbf{A}^{-1}(\mathbf{y}, x) \mathbf{B}(\mathbf{y}, x) \xi(x, \mathbf{v}) \Leftrightarrow \frac{d}{dx} \begin{bmatrix} \dot{m} \\ p_0 \\ T_0 \end{bmatrix} = - \begin{bmatrix} 0 \\ \frac{\gamma p_0 M^2 \xi}{2L} \\ 0 \end{bmatrix} \quad (12)$$

Equation (12) shows that the mass flow and the total temperature are constant through the stator cascade. As a first-order approximation and taken into account that the air injection mass flow is a very small fraction of the total mass flow, we may assume that the flow control process affects most directly the total pressure with negligible changes in the mass flow and the total temperature. Then, the momentum component of the Euler equations can be approximated as

$$\frac{1}{\alpha_i(p_{0,i})} \frac{\partial p_{0,i}}{\partial t} + \frac{\partial p_{0,i}}{\partial x} + \beta_i(p_{0,i}, M_i) \xi_i(x, \mathbf{v}) = 0 \quad (13)$$

along with the conservation of mass and energy given by

$$\dot{m}_i = \sqrt{\frac{\gamma}{RT_{0,i}}} p_{0,i} A_i M_i \left( 1 + \frac{\gamma-1}{2} M_i^2 \right)^{-\frac{k+1}{2(k-1)}} \quad (14)$$

where  $\dot{m}_i$  and  $T_{0,i}$  are constant at each radial station, denoted by the subscript  $i$ , and

$$\alpha_i = u_i \left[ 1 - \frac{(\gamma-1)T_i}{T_{0,i}} \right] \quad (15)$$

$$\beta_i = \frac{\gamma p_{0,i} M_i^2}{2L} \quad (16)$$

Let  $x = 0$  be the coordinate at the cascade inlet and  $x = L$  be the coordinate at the outlet, then the boundary condition for Eq. (13) is imposed by the inlet total pressure  $p_{0,1}$  as

$$p_{0,i}(0, t) = p_{0,1,i} \quad (17)$$

### C. Adaptive Parameter Estimation

The total pressure loss parameter  $\xi$  in Eq. (6) models the total pressure loss in the compressor cascade. For air injection control, we postulate that this total pressure loss parameter is a non-negative function of the air injection mass flow control vector  $\mathbf{v}$  that would result in a lower total pressure loss than when the air injection is not active. Thus, we have the following equation

$$\xi_i(x, \mathbf{v}) = \xi_{0,i}(x) - \Delta\xi_i(x, \mathbf{v}) \geq 0 \quad (18)$$

where  $\xi_0$  is the total pressure loss parameter before air injection control and  $0 \leq \Delta\xi \leq \xi_0$  is a total pressure loss reduction parameter due to air injection mass flow.

The LSAC experimental data are used to establish the relationship between the air injection mass flow control and the total pressure loss reduction parameter  $\Delta\xi_i$ . The experimental data indicate that the total pressure loss reduction parameter  $\Delta\xi$  could be approximated as a quadratic function of the air injection mass flow control. Hence, we select the following functional form for estimating the total pressure loss relationship as a quadratic function of the air injection mass flow control

$$\Delta\xi_i(x_i, \mathbf{v}) = \sum_{j=1}^N w_{ij} \left( \frac{2v_j v_{sat,j} - v_j^2}{v_{sat,j}^2} \right) \quad (19)$$

for  $l \leq x \leq L$  where  $x = l$  is the coordinate of the air injection location at the  $i$ -th blade radial station on the stator blade taken to be 35% of chord,  $w_{ij}$  is a weight, and  $0 \leq v_j \leq v_{sat,j}$  is an air injection mass flow where  $v_{sat,j}$  is the saturation mass flow of the  $j$ -th air injection actuator.

Equation (19) can also be written as

$$\Delta\hat{\xi}_i = \mathbf{w}_i^T \boldsymbol{\theta} \quad (20)$$

where  $\mathbf{w}_i$  is a weight matrix for the  $i$ -th air injection actuator to be estimated from measurements,  $\boldsymbol{\theta}$  is a quadratic basis function vector, and the hat symbol denotes an estimated quantity.

The total pressure loss reduction parameter  $\Delta\xi$  is computed from the total pressure loss coefficient measurements as

$$\Delta\xi_i = K \Delta\bar{\omega}_{1,i} \quad (21)$$

where  $\Delta\bar{\omega}_1$  is the average total pressure loss reduction coefficient due to air injection defined as

$$\Delta\bar{\omega}_{1,i} = \frac{\Delta p_{0,2,i}}{p_{0,1,i} - p_{1,i}} \quad (22)$$

and  $K$  is a coefficient defined as

$$K = \frac{2L(p_{0,1,i} - p_{1,i})}{\int_1^L p_{0,i} M_i^2 dx} \quad (23)$$

The coefficient  $K$  in Eq. (21) is computed off-line by interpolation as a function of the measured total pressure loss coefficient  $\bar{\omega}_1$  before the air injection actuation. To enable this computation, Eq. (12) is solved for various values of  $\xi_0$  which correspond to different values of  $\bar{\omega}_1$ . This coefficient turns out to be nearly constant with a value of 2.320.

The weighting matrix can be estimated on-line using a recursive least-squares algorithm to continuously refine the estimation based on past  $n$  data samples. The adaptive weight update law is

$$\mathbf{w}_i(k) = \mathbf{w}_i(k-1) + \mathbf{K}(k) [\mathbf{d}(k) - \boldsymbol{\theta}^T(k) \mathbf{w}_i(k-1)] \quad (24)$$

where  $k$  denotes the update cycle that repeats every  $n$  data samples,  $\mathbf{d}$  is a measurement data matrix

$$\mathbf{d}(k) = \begin{bmatrix} \Delta\xi_1(kn-n+1) & \Delta\xi_2(kn-n+1) & \cdots & \Delta\xi_N(kn-n+1) \\ \Delta\xi_1(kn-n+2) & \Delta\xi_2(kn-n+2) & & \vdots \\ \vdots & & \ddots & \Delta\xi_N(kn-1) \\ \Delta\xi_1(kn) & \cdots & \Delta\xi_{N-1}(kn) & \Delta\xi_N(kn) \end{bmatrix} \quad (25)$$

and  $\mathbf{K}$  is an adaptive gain matrix defined as

$$\mathbf{K}(k) = \mathbf{P}^{-1}(k) \boldsymbol{\theta}(k) \quad (26)$$

where

$$\mathbf{P}(k) = \Gamma^{\frac{1}{k-1}} \mathbf{P}(k-1) + \boldsymbol{\theta}(k) \boldsymbol{\theta}^T(k) \quad (27)$$

$$\boldsymbol{\theta}(k) = \begin{bmatrix} \theta_1(kn-n+1) & \theta_1(kn-n+2) & \cdots & \theta_1(kn) \\ \theta_2(kn-n+1) & \theta_2(kn-n+2) & & \vdots \\ \vdots & & \ddots & \theta_{N-1}(kn) \\ \theta_N(kn-n+1) & \cdots & \theta_N(kn-1) & \theta_N(kn) \end{bmatrix} \quad (28)$$

and  $0 \leq \Gamma \leq 1$  is a forgetting factor that is used to weigh past information.

During an on-line air injection control, the computation uses recently available total pressure loss data and the air injection mass flow input at previous  $n$  time steps to revise the initial estimate of the total pressure loss reduction parameter. This information is then used to compute an air injection control reference command signal. This process is then repeated for every  $n$  numbers of time steps until a desired total pressure at the outlet is achieved. To minimize the effect of changing inlet flow conditions, a feedback control is implemented to minimize a deviation from the air injection reference command.

The quadratic basis function provides a good approximation of the effectiveness of air injection on the reduction of the total pressure loss in the LSAC flow control experiment as shown in Fig. 15. The least-squares method in effect provides a noise filtering of the measurements. This filtering potentially prevents a potential over-identification of the total pressure reduction parameter that could result in an erroneous computation of the air injection mass flow if a higher-order polynomial were to be used as a basis function.

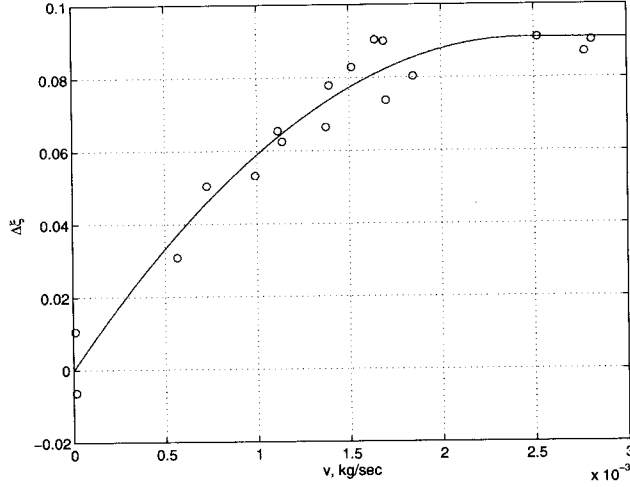


Fig. 15 - Total Pressure Loss Reduction Parameter Estimation

## V. Feedback Optimal Flow Control

The objective of the feedback flow control is to track a reference command of the air injection mass flow by compensating for changes in the inlet flow conditions which act as disturbances to the flow through the stator cascade. To form a reference command, we first compute a desired air injection mass flow to achieve a desired total pressure at the outlet of the stator cascade. Let  $p_{0,2,d}$  be the desired outlet total pressure, then the change in the outlet total pressure is  $\Delta p_{0,2} = p_{0,2} - p_{0,2,d}$ . The corresponding total pressure loss reduction parameter  $\Delta \xi_{i,d}$  at each radial station can then be computed from Eqs. (21) and (22). The recursive least-squares parameter estimation results in

$$\begin{bmatrix} \Delta \xi_{1,d} \\ \Delta \xi_{2,d} \\ \vdots \\ \Delta \xi_{N,d} \end{bmatrix} = \begin{bmatrix} w_{11} & w_{12} & \cdots & w_{1N} \\ w_{21} & w_{22} & & \vdots \\ \vdots & & \ddots & w_{N-1,n} \\ w_{N,1} & \cdots & w_{N,N-1} & w_{NN} \end{bmatrix} \begin{bmatrix} \frac{2v_{1,d}v_{sat,1} - v_{1,d}^2}{v_{sat,1}^2} \\ \frac{2v_{2,d}v_{sat,2} - v_{2,d}^2}{v_{sat,2}^2} \\ \vdots \\ \frac{2v_{N,d}v_{sat,N} - v_{N,d}^2}{v_{sat,N}^2} \end{bmatrix} \quad (29)$$

The desired air injection mass flow  $v_{i,d}$  can be computed by inverting Eq. (29) with known weights  $w_{ij}$  estimated from the recursive least-squares parameter estimation. Next, we define a reference command of the air injection mass flow based on the desired air injection mass flow. Since the air injection mass flow is delivered by a flow control valve, the actuator dynamics of the flow control valve should be incorporated into the reference command in order to ensure that the air injection mass flow is dynamically achievable. There are various types of flow control valves. Among these, the proportional type can deliver a continuous variable mass flow. The ability to control the air injection mass flow at a variable set point provides a flexibility in developing an effective flow control strategy. Typically, the actuator dynamics of a flow control valve may be described by a second-order model. In this case, the reference command has the following open-loop response

$$V_i(s) = \frac{bv_{i,d}}{s^2 + 2\zeta\omega_n s + \omega_n^2} \quad (30)$$

where  $V(s)$  is the Laplace transform of the air injection mass flow output  $v_i(t)$ ,  $\zeta$  and  $\omega_n$  are the damping ratio and the frequency of the flow control valve.

The reference command of the air injection mass flow is then used to compute a reference trajectory of the total pressure  $p_0(x,t)$  from Eq. (13) that the air injection would be able to achieve. A simple finite-difference upwind method can easily be implemented as a computational procedure for Eq. (13).<sup>13</sup> If the inlet flow condition is changing, this trajectory is likely to deviate and therefore results in the desired outlet total pressure not being met. An error signal is formed by subtracting the total pressure measurements from the reference trajectory. If we assume that the error

signal is small, then Eq. (13) can be linearized as

$$\frac{1}{\alpha_i} \frac{\partial \Delta p_{0,i}}{\partial t} + \frac{\partial \Delta p_{0,i}}{\partial x} + a_i \Delta p_{0,i} + \sum_{j=1}^N b_{ij} \Delta v_j + c_i q_i = 0 \quad (31)$$

subject to the boundary condition

$$\Delta p_{0,i}(0, t) = \Delta p_{0,1,i} \quad (32)$$

where  $\Delta p_0$  is the total pressure error,  $\Delta v$  is the air injection control augmentation,  $\Delta p_{0,1}$  is a perturbation in the inlet total pressure as a disturbance,  $a$  and  $b$  are computed as

$$a_i(x, t) = -\frac{\gamma M_i^2 (1 + \gamma M_i^2) \xi_i}{2L_i (1 - M_i^2)} \quad (33)$$

$$b_{ij}(x, t) = \begin{cases} 0 & 0 \leq x < l \\ -2\beta_i w_{ij} \frac{v_{sat,j} - v_j}{v_{sat,j}^2} & l \leq x \leq L \end{cases} \quad (34)$$

$$c_i(x, t) = \frac{\gamma p_{0,i} M_i^2 (1 + \frac{\gamma-1}{2} M_i^2) \xi_i}{L_i (1 - M_i^2)} \quad (35)$$

and  $q$  is a disturbance due to perturbations in the mass flow and total temperature defined as

$$q_i = \frac{\Delta \dot{m}_i}{\dot{m}_i} + \frac{\Delta T_{0,i}}{2T_{0,i}} \quad (36)$$

To simplify the index notation for the blade radial stations, we express Eq. (31) in a vector form as

$$\boldsymbol{\alpha}^{-1} \frac{\partial \Delta \mathbf{p}_0}{\partial t} + \frac{\partial \Delta \mathbf{p}_0}{\partial x} + \mathbf{a} \Delta \mathbf{p}_0 + \mathbf{b} \Delta \mathbf{v} + \mathbf{c} \mathbf{q} = \mathbf{0} \quad (37)$$

where  $\boldsymbol{\alpha} = \text{diag}(\alpha_i)$ ,  $\mathbf{a} = \text{diag}(a_i)$ ,  $\mathbf{b} = [b_{ij}]$ , and  $\mathbf{c} = \text{diag}(c_i)$ .

To design a feedback flow control algorithm, we will develop a linear-quadratic optimal control theory for Eq. (37) with the following cost function to minimize the outlet total pressure error  $\Delta \mathbf{p}_{0,2}$  and the air injection control augmentation  $\Delta \mathbf{v}$

$$J = \frac{1}{2} \int_t^{t+n\Delta t} (\Delta \mathbf{p}_{0,2}^T \mathbf{Q} \Delta \mathbf{p}_{0,2} + \Delta \mathbf{v}^T \mathbf{R} \Delta \mathbf{v}) dt \quad (38)$$

where  $\mathbf{Q} \geq \mathbf{0}$  and  $\mathbf{R} > \mathbf{0}$  are state and control weight matrices.

The optimality of this system has been studied for the case with only a single air-injection actuator.<sup>14</sup> The optimality conditions result in the following adjoint equation

$$\frac{\partial \boldsymbol{\lambda}}{\partial t} + \frac{\partial}{\partial x} (\boldsymbol{\alpha} \boldsymbol{\lambda}) - \mathbf{a} \boldsymbol{\alpha} \boldsymbol{\lambda} = \mathbf{0} \quad (39)$$

subject to a boundary condition  $\boldsymbol{\alpha} \boldsymbol{\lambda}(L, t) = \mathbf{Q} \Delta \mathbf{p}_{0,2}$  and the optimal control

$$\mathbf{R} \Delta \mathbf{v} - \int_0^L \mathbf{b}^T \boldsymbol{\alpha} \boldsymbol{\lambda} dx = \mathbf{0} \quad (40)$$

To derive a feedback control, we assume an adjoint solution in the form of a linear combination of the total pressure error  $\Delta \mathbf{p}_0$ , the air injection control augmentation  $\Delta \mathbf{v}$ , and the disturbance  $\mathbf{q}$

$$\boldsymbol{\alpha} \boldsymbol{\lambda}(x, t) = \mathbf{A}(x, t) \Delta \mathbf{p}_0(x, t) + \mathbf{B}(x, t) \Delta \mathbf{v} + \mathbf{C}(x, t) \mathbf{q} \quad (41)$$

where  $\mathbf{A} = \text{diag}(A_i)$ ,  $\mathbf{B} = [B_{ij}]$ , and  $\mathbf{C} = \text{diag}(C_i)$ .

Substituting this into Eqs. (39) and (31) and neglecting the time derivative terms, which in essence gives rise to a quasi-steady state solution, we obtain the following partial differential equations

$$\frac{\partial \mathbf{A}}{\partial x} = \mathbf{a} \mathbf{A} + \mathbf{A} \mathbf{a} \quad (42)$$

$$\frac{\partial \mathbf{B}}{\partial x} = \mathbf{aB} + \mathbf{Ab} \quad (43)$$

$$\frac{\partial \mathbf{C}}{\partial x} = \mathbf{aC} + \mathbf{Ac} \quad (44)$$

subject to corresponding boundary conditions  $\mathbf{A}(L, t) = \mathbf{Q}$ ,  $\mathbf{B}(L, t) = \mathbf{0}$ , and  $\mathbf{C}(L, t) = \mathbf{0}$ .

Similarly, we assume a solution for Eq. (31)

$$\Delta \mathbf{p}_0(x, t) = \mathbf{D}(x, t) \Delta \mathbf{p}_{0,2} + \mathbf{E}(x, t) \Delta \mathbf{v} + \mathbf{F}(x, t) \mathbf{q} \quad (45)$$

where  $\mathbf{D} = \text{diag}(D_i)$ ,  $\mathbf{E} = [E_{ij}]$ , and  $\mathbf{F} = \text{diag}(F_i)$ .

Substituting this into Eq. (31) and again neglecting the time derivative term, we obtain the following partial differential equations

$$\frac{\partial \mathbf{D}}{\partial x} = -\mathbf{aD} \quad (46)$$

$$\frac{\partial \mathbf{E}}{\partial x} = -\mathbf{aE} - \mathbf{b} \quad (47)$$

$$\frac{\partial \mathbf{F}}{\partial x} = -\mathbf{aF} - \mathbf{c} \quad (48)$$

subject to corresponding boundary conditions  $\mathbf{D}(L, t) = \mathbf{I}$ ,  $\mathbf{E}(L, t) = \mathbf{0}$ , and  $\mathbf{F}(L, t) = \mathbf{0}$ .

We let  $x = 0$  in Eq. (45) and then proceed to solve for the air injection control augmentation  $\Delta \mathbf{v}$  as

$$\Delta \mathbf{v} = \mathbf{E}^{-1}(0, t) [\Delta \mathbf{p}_{0,1} - \mathbf{D}(0, t) \Delta \mathbf{p}_{0,2} - \mathbf{F}(0, t) \mathbf{q}] \quad (49)$$

Substituting Eq. (49) back into Eq. (45) results in

$$\Delta \mathbf{p}_0(x, t) = \mathbf{E}(x, t) \mathbf{E}^{-1}(0, t) \Delta \mathbf{p}_{0,1} + [\mathbf{D}(x, t) - \mathbf{E}(x, t) \mathbf{E}^{-1}(0, t) \mathbf{D}(0, t)] \Delta \mathbf{p}_{0,2} + [\mathbf{F}(x, t) - \mathbf{E}(x, t) \mathbf{E}^{-1}(0, t) \mathbf{F}(0, t)] \mathbf{q} \quad (50)$$

Upon further substituting Eq. (50) into Eq. (39), we get

$$\alpha \lambda(x, t) = \mathbf{A}(x, t) \mathbf{E}(x, t) \mathbf{E}^{-1}(0, t) \Delta \mathbf{p}_{0,1} + \mathbf{A}(x, t) [\mathbf{D}(x, t) - \mathbf{E}(x, t) \mathbf{E}^{-1}(0, t) \mathbf{D}(0, t)] \Delta \mathbf{p}_{0,2} + \mathbf{B}(x, t) \Delta \mathbf{v} + \{\mathbf{A}(x, t) [\mathbf{F}(x, t) - \mathbf{E}(x, t) \mathbf{E}^{-1}(0, t) \mathbf{F}(0, t)] + \mathbf{C}(x, t)\} \mathbf{q} \quad (51)$$

The optimal control in Eq. (40) can now be obtained as a feedback on the outlet total pressure error and a disturbance feedforward on changes in the inlet flow condition

$$\Delta \mathbf{v} = \mathbf{K}_1 \Delta \mathbf{p}_{0,1} + \mathbf{K}_2 \Delta \mathbf{p}_{0,2} + \mathbf{K}_q \mathbf{q} \quad (52)$$

where  $\mathbf{K}_1$ ,  $\mathbf{K}_2$ ,  $\mathbf{K}_q$  are the optimal control gain matrices defined as

$$\mathbf{K}_1(t) = \left[ \mathbf{R} - \int_0^L \mathbf{b}^T \mathbf{B}(x, t) dx \right]^{-1} \int_0^L \mathbf{b}^T \mathbf{A}(x, t) \mathbf{E}(x, t) \mathbf{E}^{-1}(0, t) dx \quad (53)$$

$$\mathbf{K}_2(t) = \left[ \mathbf{R} - \int_0^L \mathbf{b}^T \mathbf{B}(x, t) dx \right]^{-1} \int_0^L \mathbf{b}^T \mathbf{A}(x, t) [\mathbf{D}(x, t) - \mathbf{E}(x, t) \mathbf{E}^{-1}(0, t) \mathbf{D}(0, t)] dx \quad (54)$$

$$\mathbf{K}_q(t) = \left[ \mathbf{R} - \int_0^L \mathbf{b}^T \mathbf{B}(x, t) dx \right]^{-1} \int_0^L \mathbf{b}^T \{\mathbf{A}(x, t) [\mathbf{F}(x, t) - \mathbf{E}(x, t) \mathbf{E}^{-1}(0, t) \mathbf{F}(0, t)] + \mathbf{C}(x, t)\} dx \quad (55)$$

To ensure a non-singular optimal control, we must limit the value of the control weight matrix  $\mathbf{R}$  such that

$$\mathbf{R} \neq \int_0^L \mathbf{b}^T \mathbf{B}(x, t) dx \quad (56)$$

From Eq. (52), it can be seen that the control augmentation  $\Delta v$  is a feedback optimal control of the outlet total pressure error  $\Delta p_{0,2}$  as well as the disturbances due to changes in the inlet flow conditions  $\Delta p_{0,1}$  and  $q$ . Since the one-dimensional flow model is continuous with respect to  $x$ , the optimal flow control theory in effect transforms a control that would have to depend on a continuous distribution of the total pressure error along the stator cascade as defined by Eq. (37) into one that only depends on the flow quantities at the stator inlet and outlet. The distribution is integrated out in the gain matrices. In contrast, a conventional feedback control method could be used by decomposing the partial differential equation (37) into a series of ordinary differential equations in a standard state space form. A standard linear-quadratic regulator (LQR) optimal control method<sup>15</sup> could then be implemented but would require the total pressure error distribution along the stator flow passage to be measured or estimated. The implementation of such a method is inherently more complex than the present feedback optimal flow control approach. Fig. 16 illustrates a block diagram of the present feedback optimal flow control approach.

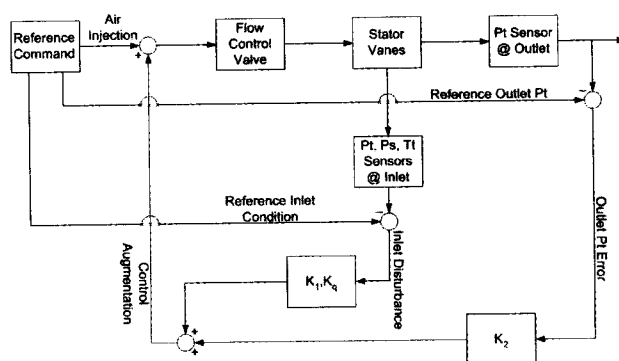


Fig. 16 - Feedback Optimal Flow Control Block Diagram

## VI. Simulation Results and Discussion

To demonstrate the present flow control concept, a flow control simulation is performed. We consider the LSAC stator blades to be equipped with sensors and air injection actuators at five different radial stations. Table 1 shows the pertinent information of the blade sections at these radial stations in terms of the camber angle  $\theta$ , stagger angle  $\zeta$ , thickness-to-chord ratio  $t/c$ , and solidity  $\sigma$ . The inlet total pressure is assumed to be uniform at a value of 2110 psf with a Mach number of 0.3 corresponding to the LSAC flow conditions. The air approaches the stator with an inlet air angle  $\beta_1$  as shown in Table 1.

$i$	$(r - r_h) / (r - r_t)$	$\theta$	$\zeta$	$t/c$	$\sigma$	$\beta_1$	$\bar{\omega}_1$
1	0.117	43.55	36.34	0.0623	1.506	61.01	0.1573
2	0.331	40.11	32.05	0.0695	1.431	56.04	0.1050
3	0.513	39.00	31.34	0.0756	1.383	54.81	0.0955
4	0.684	39.43	32.06	0.0813	1.351	55.19	0.0970
5	0.885	44.97	38.31	0.0872	1.335	60.94	0.1520

Table 1 - LSAC Blade Radial Stations

The performance of this cascade is then predicted by a NACA 65-series cascade correlation method based on the Carter's rule

$$\Delta\beta = \beta_1 - \beta_2 = i_0 - \delta_0^0 + \theta(1 - m + n) \quad (57)$$

where  $\Delta\beta$  is the turning angle,  $i_0$  is the reference minimum-loss incidence angle,  $\delta_0^0$  is the reference deviation angle at the reference incidence angle, and  $m$  and  $n$  are the slope parameters as functions of the inlet air angle  $\beta_1$  and the solidity  $\sigma$ .<sup>9</sup>

The predicted outlet air angle  $\beta_2$  is then used to compute the diffusion factor according to Eq. (4). The total pressure loss coefficient  $\bar{\omega}_1$  is then estimated from the diffusion factor correlation according to Fig. 17, which has

been adjusted from Fig. 11 in order to account for secondary losses since the total pressure losses from Fig. 11 are associated with two-dimensional blade sections. As can be seen, with air injection off, the diffusion factor is as high as 0.66 in the hub and tip regions and is as low as 0.58 in the mid span blade station. This is indicative of adverse flow conditions in the hub and the tip regions. To mitigate the potential flow separation, the total pressure losses through the stator cascade must be reduced. This in turn requires the diffusion factor to decrease as shown in Fig. 17. With air injection on, the diffusion factor is reduced to within a range from 0.52 at the mid-span region to 0.59 in the hub and tip regions. Due to the air injection control saturation, the diffusion factor at the hub and tip regions cannot be further reduced.

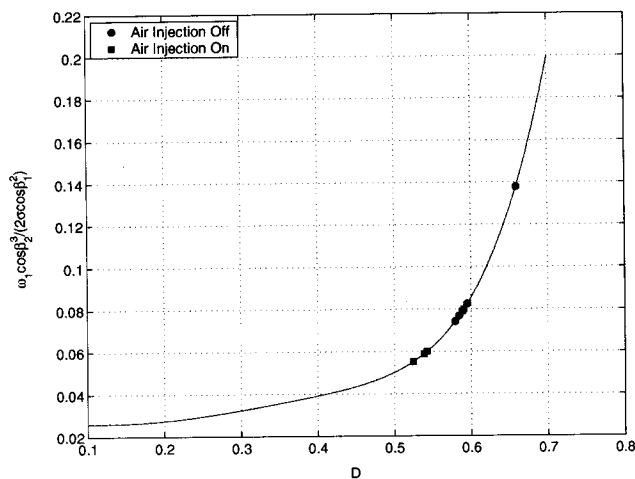


Fig. 17 - Diffusion Factor Correlation

The effect of air injection on the total pressure recovery is modeled as a two-dimensional turbulent plane jet flow<sup>8</sup> to simulate the decay in the total pressure recovery as a function of the radial displacement from the source of the air injection where its amplitude is maximum. Thus, the total pressure recovery due to the air injection is assumed to have the following profile

$$\Delta p_{0,2}(r) = \frac{\Delta \xi_i}{K} (p_{0,1,i} - p_{1,i}) e^{-c_i(r-r_i)^2} \quad (58)$$

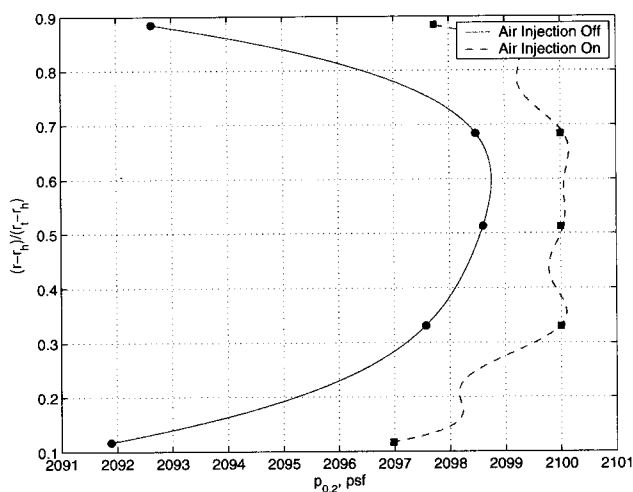


Fig. 18 - Outlet Total Pressure Profiles

Fig. 18 is a plot of the predicted outlet total pressure profiles with air injection off and on. A significant deficit in the outlet total pressure exists at the hub and tip regions due to flow separation before air injection actuation. To reduce the extent of flow separation, air injection control is activated at all five radial stations. The simulation results show an improvement in the outlet total pressure profile upon air injection activation. The total pressure deficit in the hub and tip regions is reduced and the profile in the core region also becomes more uniform. The local variation in the profile is due to the small number of the radial stations used in the simulation. The reference command of the air injection mass flow at these blade radial stations are as shown in Fig. 19. The hub and tip regions demand the highest amount of air injection due to the significant total pressure losses therein. However, the effectiveness of the air injection flow control in these regions is limited by the air injection mass flow command reaching a saturation limit.

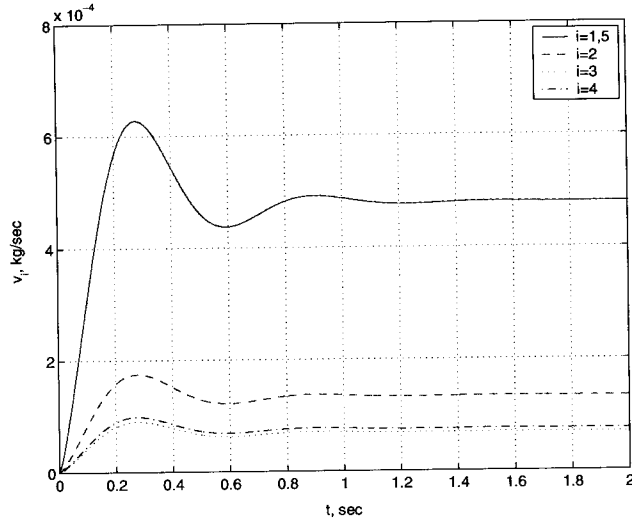


Fig. 19 - Reference Air Injection Mass Flow

To demonstrate the feedback flow control approach, we synthesize a variation in the inlet flow condition that results in an inlet Mach number perturbation of 1% and a total pressure perturbation of -0.1%. The feedback flow control is computed with weights  $Q = 1 \times 10^{-2}$  and  $\mathbf{R} = \text{diag}(10^6, 10^2, 10^2, 10^2, 10^6)$ . The high control weights at the hub and tip regions are required since the air injection mass flow is much higher than the air injection mass flow in the core region. The effectiveness of the feedback flow control in the mid-span and hub regions are illustrated in Figs. 20 and 21, respectively.

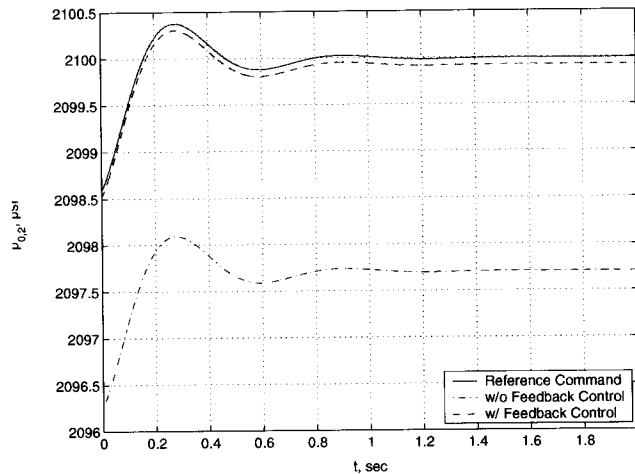


Fig. 20 - Feedback Control Tracking at Mid-Span Radial Station  $i = 3$

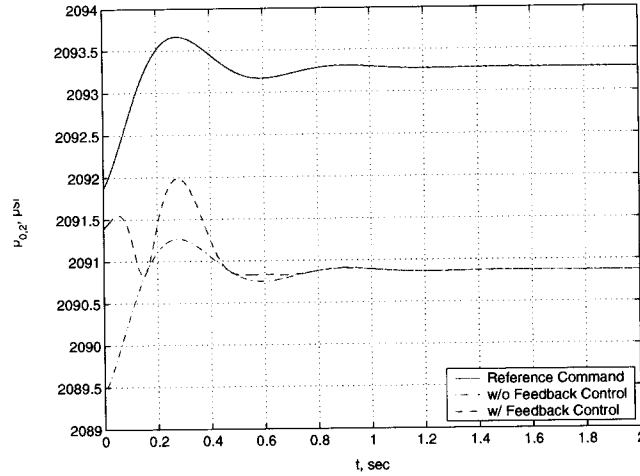


Fig. 21 - Feedback Control Tracking at Hub Radial Station  $i = 1$

As can be seen, the feedback control augmentation at the mid-span radial station  $i = 3$  is capable of tracking the reference trajectory of the outlet total pressure reasonably well. Without the feedback flow control, the desired outlet total pressure is not achievable. A very small steady state error exists as a result of the lack of an integral feedback in the flow control design. In contrast, the feedback control augmentation at the hub radial station  $i = 1$  is not at all effective in tracking the reference command. This is simply due to the fact that the air injection mass flow at the hub is already at a saturation limit, so any additional control will not be able to reduce the total pressure losses further.

Fig. 22 is a plot of the air injection mass flow control augmentation obtained from the feedback control. In the hub and tip regions, the augmented air injection mass flow is essentially zero, indicating that the air injection flow control has reached a saturation limit. In the core region, the augmented air injection mass flow is positive, indicating an additive air injection effect to compensate for the total pressure decrease at the inlet.

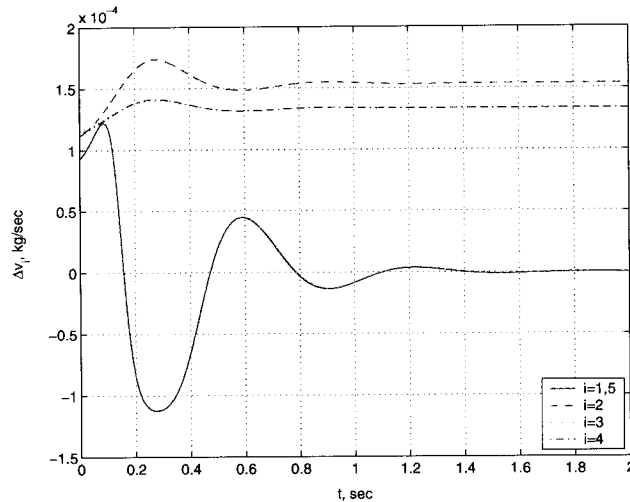


Fig. 22 - Air Injection Mass Flow Control Augmentation

It should be noted that in the present flow control method, we have not considered the effect of line loss in the pressure tubing. In practice, this effect can potentially limit the overall performance of the flow control design. If the pressure tubing from the bleed air reservoir is significantly long, the mass flow will likely be throttled down due to the line loss effect. This would potentially result in an under-actuated control whereby the flow control valve would not be able to deliver the correct air injection mass flow. Moreover, the line loss effect also causes a time delay in the

delivery of the air injection mass flow. Therefore, it is important that the pressure tubing be kept as short as possible in order to maintain a proper performance of the flow control.

The issue of sensor placements is critical in designing an effective flow control. Real flow in a compressor cascade exhibits a tangential variation. Since the pressure loss parameter is determined from the tangentially average total pressure quantities, the cascade flow passage at the inlet and outlet should be covered sufficiently with total pressure sensors. Alternatively, a single sensor could be placed at a strategic location that allows it to measure a local total pressure quantity that is approximately equal to the tangentially average total pressure quantity. Fig. 23 shows a sample of three tangential variations of the total pressure measurements normalized to the flow-weighted tangentially average total pressure at the stator inlet and outlet in the LSAC test facility. The abscissa  $n\theta/2\pi$  is the tangential coordinate of the flow passage around one stator blade with  $0 \leq n\theta/2\pi < 1/2$  being the flow region below the pressure surface. As can be seen, the total pressure at the outlet exhibits a sharp wake at the trailing edge. Based on these total pressure profiles, it appears that a single total pressure sensor could be placed at  $n\theta/2\pi \approx 0.32$  at the inlet and the outlet where the local total pressure is about equal to the average total pressure. The advantage of a single sensor location is the simplicity in the sensing method that would eliminate the needs for computing the tangentially average total pressure. This in turn would reduce the computational overhead in the feedback flow control implementation.

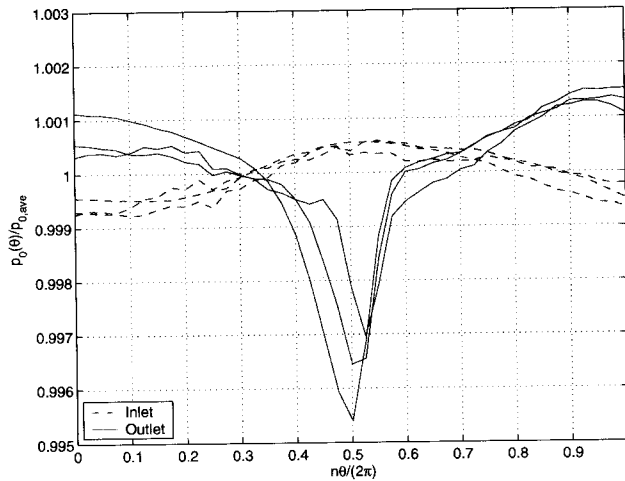


Fig. 23 - Tangential Variations of Total Pressure at Stator Inlet and Outlet

## VII. Conclusions

This study has presented an optimal flow control method using air injection as a means for flow separation control in a stator cascade of a low-speed axial flow compressor. Experimental testing in the Low Speed Axial-Flow Compressor (LSAC) test facility at NASA Glenn Research Center has shown the effectiveness of air injection in reducing the total pressure losses associated with flow separation. A multi-sensor, multi-actuator flow control approach is introduced whereby the total pressure losses at the sensing stations are monitored. Air injection actuators are activated whenever the total pressure losses exceed a prescribed limit. A model-based feedback flow control method is developed based on a one-dimensional model of the flow through a stator cascade. The model incorporates a total pressure loss parameter that accounts for viscous losses associated with flow separation in a compressor cascade. An adaptive parameter estimation is developed using a recursive least-squares algorithm with a quadratic basis function to perform an on-line estimation of the total pressure loss parameter. The feedback flow control is derived from an adjoint optimal control method to enable a feedback from the outlet total pressure error and a disturbance feedforward to handle changes in the inlet flow condition. A simulation shows that the feedback flow control method is effective in controlling the outlet total pressure due to flow disturbances at the stator inlet.

## References

- <sup>1</sup>Lord, W. K., MacMartin, D. G., and Tillman, T. G., "Flow Control Opportunities in Gas Turbine Engines", *AIAA Fluids Conference*, AIAA-2000-2234, June 2000.
- <sup>2</sup>MacMartin, D. G., Murray, R. M., Verma, A., and Paduano, J. D., "Active Control of Integrated Inlet/Compression Systems: Initial Results", *2001 ASME Fluids Engineering Division Summer Meeting*, FEDSM2001-18275, June 2001.
- <sup>3</sup>Leinhos, D. C., Scheidler, S. G., and Fottner, L., "Experiments in Active Stall Control of a Twin-Spool Turbofan Engine", *Proceedings of ASME TURBO EXPO 2002*, GT-2002-30002, June 2002.
- <sup>4</sup>d'Andrea, R., Behnken, R. L., and Murray, R. M., "Active Control of an Axial Flow Compressor via Pulsed Air Injection", *California Institute of Technology CDS Report 95-029*, July 1996.
- <sup>5</sup>Culley, D. E., Bright, M. M., Prahst, P. S., and Strazisar, A. J., "Active Flow Separation Control of a Stator Vane Using Surface Injection in a Multistage Compressor Experiment", *Proceedings of ASME TURBO EXPO 2003*, GT2003-38863, June 2003.
- <sup>6</sup>Kim, S. H. and Kim, C., "Separation Control on NACA23012 Using Synthetic Jet", *3rd AIAA Flow Control Conference*, AIAA-2006-2853, June 2006.
- <sup>7</sup>Moore, F. K., and Greitzer, E. M., "A Theory of Post-Stall Transients in Axial Compression Systems: Part I Development of Equations", *Journal of Engineering for Gas Turbines and Power*, Vol. 108, Jan 1986.
- <sup>8</sup>Blevins, R. D., *Applied Fluid Dynamics Handbook*, Van Nostrand Company, New York, 1984.
- <sup>9</sup>National Aeronautics and Space Administration, *Aerodynamic Design of Axial-Flow Compressors*, NASA SP-36, 1965.
- <sup>10</sup>Dixon, S. L., *Fluid Mechanics - Thermodynamics of Turbomachinery*, 3rd Edition, Pergamon Press, New York, 1989.
- <sup>11</sup>Ravindran, S. S., "Reduced-Order Adaptive Controllers for Fluid Flows Using POD", *Journal of Scientific Computing*, 2000; 15(4): 457-478.
- <sup>12</sup>Shapiro, A. H., *The Dynamics and Thermodynamics of Compressible Fluid Flow*, Volume II, Ronald Press Company, New York, 1954.
- <sup>13</sup>Hirsh, C., *Numerical Computation of Internal and External Flows*, Vol. 1, John Wiley & Sons, Brussels, 1991.
- <sup>14</sup>Nguyen, N. T., Bright, M. M., Culley, D. E., "Feedback Adaptive Flow Control of Air Injection in Compressors", *AIAA Guidance, Navigation, and Control Conference*, AIAA-2005-6072, August 2005.
- <sup>15</sup>Brogan, W. L., *Modern Control Theory*, 3rd Edition, Prentice Hall, New Jersey, 1991.